Journal of Catalysis **200,** 197–202 (2001)
doi:10.1006/jcat.2001.3196, available online at http://www.idealibrary.com on IDEAL®

RESEARCH NOTE

Silica–Alumina Catalyst with Bimodal Pore Structure Prepared by Phase Separation in Sol–Gel Process

Ryoji Takahashi,[1] Satoshi Sato, Toshiaki Sodesawa, and Miyuki Yabuki

Department of Materials Technology, Faculty of Engineering, Chiba University, Yayoi, Inage, Chiba 263-8522, Japan

Received January 18, 2001; accepted February 6, 2001; published online April 18, 2001

An amorphous silica–alumina catalyst with distinct bimodal pore structure was prepared by sol–gel reactions of tetraethoxysilane (TEOS) and aluminum nitrate in the presence of poly(ethylene oxide) (PEO). It contains macropores effective for rapid molecular transportation and mesopores providing a large specific surface area of $\sim$600 $m^2 g^{-1}$. The pore size distribution of the macropores is sharp and its average diameter varies from 0.3 to 5 μm by altering the starting compositions such as water/TEOS and PEO/TEOS weight ratios. The macropores are formed when transitional morphologies of spinodal decomposition are fixed by sol–gel transition of inorganic components, and their size is controlled by altering the timing of the onset of spinodal decomposition and gelation. A change in the starting composition would affect this timing. In addition to macropores, silica–alumina has a large number of Brønsted acid sites, and shows excellent catalytic activity in the cracking of cumene. PEO would have the effect of increasing the uniformity of Al atoms in the silica network, which would be a cause of the formation of Brønsted acid sites.

Key Words: **silica–alumina; bimodal pore structure; sol–gel; spinodal decomposition; solid acid.**

INTRODUCTION

A material with both micrometer-sized macropores and nanometer-sized mesopores, i.e., with a distinct bimodal pore structure, has excellent advantages in industrial solid-catalysis reaction because the macropores provide pathways for rapid molecular transportation and the mesopores serve a large area of active surface. For example, it was shown in the 1960s that the presence of macropores of micrometer size can remarkably lower the pore diffusion resistance of N_2 and He gases in a bimodal pore pellet 0.5 in. thick prepared by compressing a powder (1). However, it has been difficult to control macropore and mesopore sizes concurrently for inorganic materials by conventional methods. Recently, Nakanishi *et al.* reported a preparation of silica with bimodal pore structure based on phase separation in a sol–gel process of silicon alkoxide in the presence of organic polymer (2, 3). Here, the macropore is formed by fixing a transitional structure of phase separation through spinodal decomposition, and the mesopore reflects the aggregation state of the gel structure (4). As a first application of the material, they prepared a column for HPLC from a rod-type silica monolith with bimodal pore structure (5). Because of the uniform pore size of interconnected macropores, the column shows superior separation properties in HPLC analysis compared with conventional packed columns. The HPLC column is now sold by Merck (Germany) as SilicaROD. Further application of the material is expected in various fields.

Incidently, amorphous silica-based mixed metal oxides such as silica–alumina and silica–zirconia are widely used as solid acid catalysts, and their acidic properties are known to vary depending on the preparation procedure (6). We have reported a preparation of silica–alumina catalysts by chemical vapor deposition (CVD), and investigated the acidic property of catalysts (7–9). The CVD method was also adopted by several researchers because simple layered structures are regarded as a model structure to explore how acid sites form on the surface of mixed metal oxides (10–13). Recently, a sol–gel process has attracted much interest as a novel method to prepare supported metal catalysts (14–17) and mixed metal oxide catalysts (18–20). In the sol–gel process, hetero-polycondensation forming a bond such as M–O–Si, where M is a metal, is expected to proceed from a homogeneous solution. Therefore, the sol–gel process is considered to be suitable to control the dispersion of metal particles in a metal–support composite (14) and the homogeneity in mixed metal oxides (18, 19). By inducing phase separation in the sol–gel preparation of catalysts to provide macropores, we will prepare attractive solid catalysts with well-designed bimodal pore structure together with active surfaces.

[1] To whom correspondence should be addressed. Fax: +81-43-290-3376. E-mail: rtaka@tc.chiba-u.ac.jp.

0021-9517/01 $35.00

In this work, we apply the macropore formation by phase separation to a silica–alumina system with 10 wt% of alumina useful as a solid acid catalyst. In addition to pore structure control, we investigate how the organic additive used to induce phase separation affects the generation of acid sites.

METHODS

The silica–alumina was prepared from tetraethyl orthosilicate (TEOS), aluminum nitrate, and poly(ethylene oxide) (PEO) with an average molecular weight (MW) of 100,000. TEOS was added into 1 mol dm^{-3} nitric acid aqueous solution containing aluminum nitrate and PEO with vigorous stirring. The starting compositions are summarized in Table 1. After the solution had become homogeneous, it was sealed in a plastic container, and kept at 50°C for 24 h for gelation. The resultant wet gel was dried at 50°C for 1 week and then heated at 600°C for 2 h. A reference silica–alumina sample was prepared from a solution without PEO (SAN1 in Table 1). For comparison, another silica–alumina sample was prepared by impregnation using CARiACT Q6 (Fuji silysia, Japan) as a support (denoted as SAimp).

A scanning electron microscope (SEM: ABT-32T, Topcom, Japan) was employed to examine the morphology of samples on a micrometer scale. The distribution of pores larger than 50 nm in diameter was measured by mercury porosimetry (Poresizer-9310, Micromeritics Co., USA). Thermal gravimetry and differential thermal analyses (TG-DTA; TGA-DTA2000, Mac Science Co., Japan) were carried out in air flow at a heating rate of 10 K min^{-1} for a sample dried at 50°C. BET surface area and total mesopore volume were calculated from a N_2 adsorption isotherm at −196°C, which was measured using an automatic adsorption-measurement system (Omnisorp100CX, Coulter, USA). Distribution of pores smaller than 50 nm was calculated from the desorption isotherm according to the Dollimore–Heal method (21). Before each N_2 adsorption, the sample was degassed at 300°C for 1 h. Temperature-programmed desorption (TPD) profiles of NH_3 and 2,6-dimethylpyridine (2,6-DMP) adsorbed at 200°C were measured with heating rate of 10 K min^{-1} and flow rate of N_2 carrier gas of 54 cm^3 min^{-1} on an apparatus equipped with an electric conductivity cell as a detector. The carrier gas with desorbed probe molecules was introduced into a dilute H_2SO_4 aqueous solution. Then, the concentration of H^+ in the solution decreases because of the neutralization reaction. The amount of probe molecules was calculated from a change in the electric conductivity of the solution. Details of the apparatus and the measurement conditions are reported elsewhere (22–24). The cracking of cumene was performed in a pulse reactor using 10 mg of catalyst and a cumene pulse size of 7.2 μmol (1 mm^3) at 300°C. Before the reaction, the catalyst had been ground into powders between 0.05 and 0.2 mm. The apparent first-order reaction rate constant was calculated from conversion of cumene according to an equation proposed by Basett and Habgood (25).

RESULTS AND DISCUSSION

Many water-soluble organic polymers have been reported to induce phase separation in sol–gel reactions of TEOS to provide a macroporous gel (4). For example, phase separation in the system with PEO is induced by a repulsive interaction between polar solvent and PEO with hydrophobic character because of interaction with silica by hydrogen bonding between the ether oxygens in PEO and silanols on the silica surface (3). There are two general types of phase separation process: spinodal decomposition and classic nucleation growth (26). The former occurs within a spinodal line (unstable region) in a phase diagram, and proceeds spontaneously as the continuous growth of a compositional fluctuation. It has been proved by time-resolved light-scattering measurement that the phase separation in sol–gel reactions proceeds through spinodal decomposition, in which a bicontinuous interconnected morphology grows continuously (4). By freezing the transitional structure of spinodal decomposition at various stages by sol–gel transition, bicontinuous structures of various size can be fixed as permanent structures. In a sol–gel-derived silica gel, macroporous morphology is stable against drying and heating at <1000°C, although a continuous decrease in domain size occurs as a result of bulk shrinkage.

In our preliminary experiment, we have found that PEO can be used to control the macroporous morphology by phase separation in the TEOS–aluminum nitrate system. Table 1 lists the obtained gels with different starting compositions, and Fig. 1 shows scanning electron micrographs of silica–alumina with macropores. The gel prepared without PEO (SAN1) is transparent and contains no macropores, while the gels prepared with PEO show a varying appearance depending on the PEO/TEOS and H_2O/TEOS weight

TABLE 1

Starting Compositions and Appearance of the Gel Samples Obtained[a]

Sample	H_2O (g)	PEO (g)	Appearance
SAO1	11.5	0.4	Two phases
SAO2	11.5	1.15	White opaque
SAO3	7.5	1.15	White opaque
SAO4	11.5	1.6	White opaque
SAO5	11.5	1.9	White opaque
SAN1	11.5	0	Transparent

[a] Other compositions were 60 wt% nitric acid aqueous solution, 1.15 g; $Al(NO_3)_3 9H_2O$, 2.21 g; TEOS, 9.31 g. (Si/Al = 7.64).

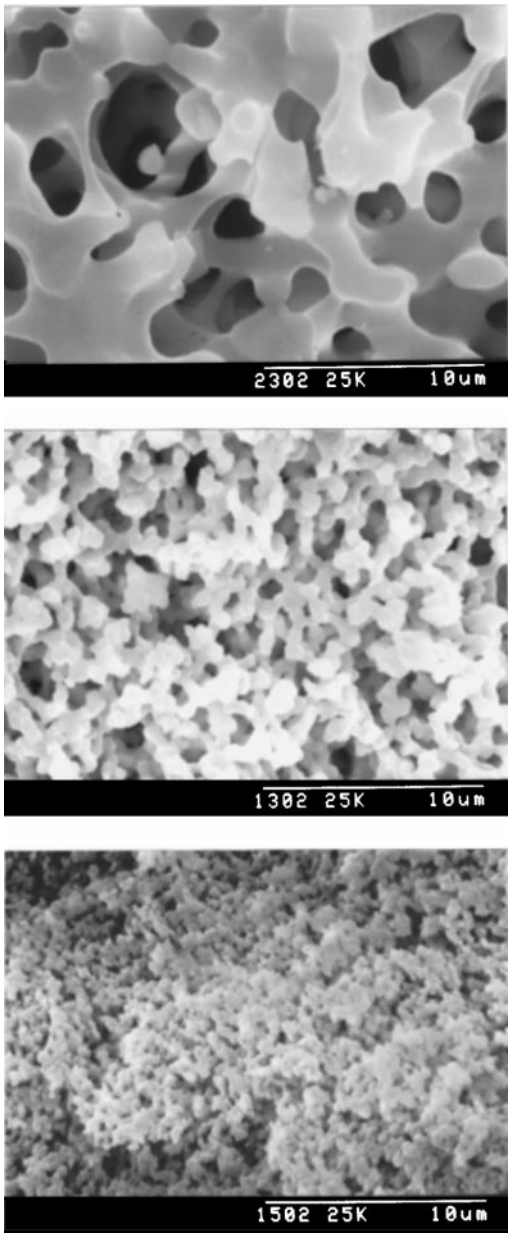

FIG. 1. Scanning electron micrographs of the fractured surface of silica–alumina samples prepared with the compositions of SAO3, SAO4, and SAO5, listed in Table 1, from the top downward.

ratios. We observe that the domain size of the gel obtained slightly increases with increasing H_2O/TEOS ratio, and decreases markedly with increasing PEO/TEOS ratio. The dependence of domain size on starting composition agrees well with that reported for the pure silica TEOS–PEO system (3). The results indicate that the addition of aluminum nitrate in the TEOS–PEO system has little influence on the type of morphology that forms via spinodal decomposition. Thus, we can control the domain size of macropore in the silica–alumina system with PEO as shown in Fig. 1.

Figure 2 shows TG-DTA profiles of the SAO3 sample dried at 50°C. In addition to an endothermic weight loss at 100°C, an exothermic weight loss, attributed to the burning of PEO, is detected at 200–300°C in the dried sample. Although most of the organic additives are removed at <300°C, the samples calcined at 500°C for 2 h are dark in color, apparently due to organic residues. White samples without organic residues were obtained by heating at 600°C. The slight weight loss over 600°C would be attributed to the elimination of H_2O by the formation of Si–O–Si bonds from silanols.

Figure 3 shows N_2 adsorption isotherms of SAO3 samples calcined at 600 and 800°C. The sample calcined at 600°C shows relatively large N_2 uptakes. The hysteresis behavior at P/P_0 values of 0.4–0.5 suggests the existence of mesopores. By calcination at 800°C, the amount of adsorption of N_2 somewhat decreases because of the collapse of mesopores. However, the difference in macropore structure between the samples calcined at 600 and 800°C is barely detectable except for a small decrease in macropore size.

Structural features obtained from N_2 adsorption measurements are summarized in Table 2, together with those obtained by other methods. All the silica–alumina samples prepared by sol–gel processes show similar average mesopore diameters (~2.5–3.5 nm), and the samples prepared with PEO, which also contain macropores, show larger BET surface areas of ~600 $m^2\ g^{-1}$. Figure 4 shows pore size distributions for the samples whose morphologies are shown in Fig. 1. Pores in the micrometer, $0.3 < D < 5\ \mu$m, and the

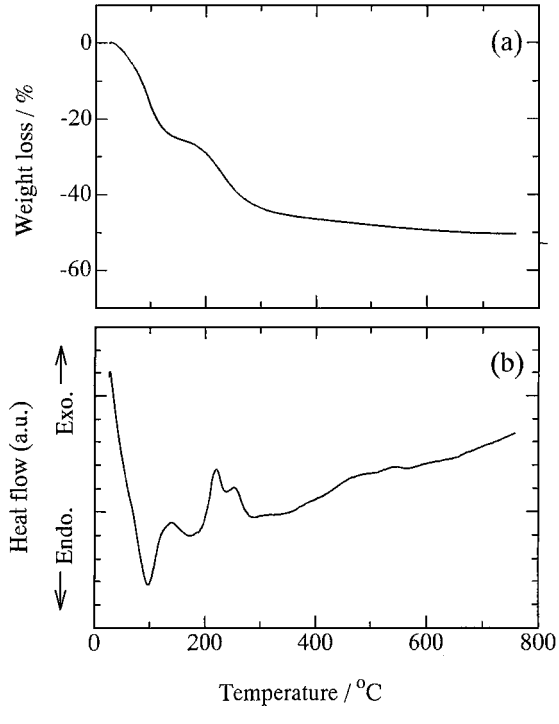

FIG. 2. TG (a) and DTA (b) profiles of SAO3 sample dried at 50°C.

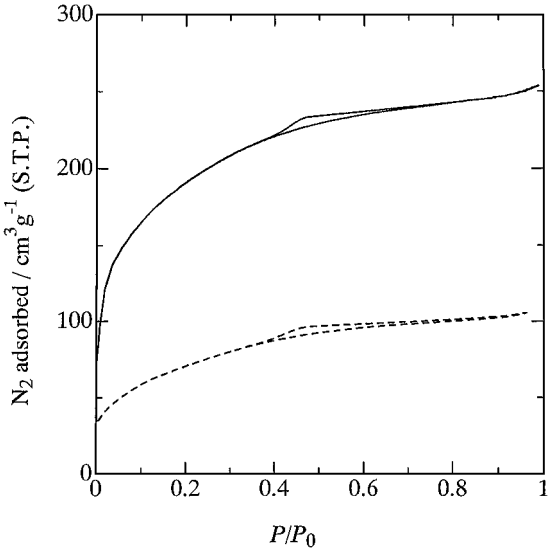

FIG. 3. N_2 adsorption isotherms of SAO3 samples calcined at 600°C (solid line) and 800°C (dotted line).

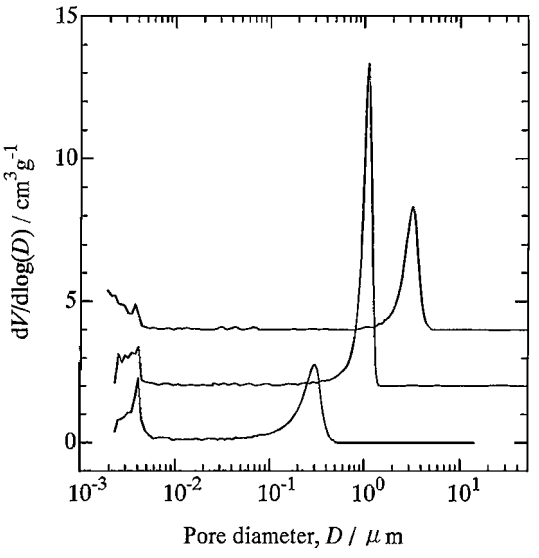

FIG. 4. Pore size distributions of silica–alumina samples prepared with the compositions of SAO3, SAO4, and SAO5, from the top downward. Pores smaller than 50 nm were measured by N_2 adsorption, and those larger than 50 nm were measured by mercury porosimetry.

nanometer, $D < 5$ nm, ranges are present. The size of the macropore agrees with that observed in the scanning electron micrograph for each sample; the pore structure in the nanometer range is very similar in all samples.

Figure 5 shows the TPD profiles of NH_3 and 2,6-DMP adsorbed on the sample of SAO3 at 200°C. Most of the adsorbed probe molecules desorb below 600°C. The total amounts of NH_3 and 2,6-DMP adsorbed are given in Table 2. The samples prepared by the sol–gel method show large amounts of adsorption for both NH_3 and 2,6-DMP, while those prepared using PEO show even larger values. The differences in the amount of adsorbed probe molecules are very significant for 2,6-DMP adsorption. Because of steric hindrance by methyl groups, 2,6-DMP adsorbs only on Brønsted acid sites, in contrast to NH_3, which adsorbs on both Lewis and Brønsted acid sites (22). It appears that the silica–alumina prepared by the sol–gel process has a larger amount of Brønsted acid sites than that prepared by impregnation, most likely because of the higher homogeneity of the Al atoms in the silica network.

In addition, the TPD results indicate that PEO has the ability to generate more Brønsted acid sites on the surface of silica–alumina. As described above, PEO forms hydrogen bonds with silica in sol–gel reactions. The interaction between PEO and silica not only induces the phase separation, but also affects the condensation pathways of silica polymers and the mesopore structure in the calcined gel (27–29). In addition, the oxygens in the PEO can coordinate with Al^{3+} cations. This coordination probably affects the homogeneity in silica–alumina and the local

TABLE 2

Structural and Catalytic Properties of Silica–Alumina Samples

Sample	SA[a] ($m^2 g^{-1}$)	PV_{meso}[b] ($cm^3 g^{-1}$)	PD_{meso}[c] (nm)	PV_{macro}[d] ($cm^3 g^{-1}$)	PD_{macro}[e] (μm)	NH_3[f] (μmol g^{-1})	2,6-DMP[f] (μmol g^{-1})	$k' \times 10^7$[g] (mol $Pa^{-1} g^{-1} min^{-1}$)
SAO3	620	0.388	2.5	0.87	3.6	250	205	308
SAO4	606	0.434	2.9	1.5	1.2	240	180	252
SAO5	635	0.557	3.5	0.77	0.3	245	190	283
SAN1	536	0.358	2.7	0	0	195	100	79
SAimp	440	0.769	7	0	0	105	33	7

[a] Specific surface area calculated by BET method.
[b] Volume of pores smaller than 50 nm in diameter.
[c] Average pore diameter calculated as $4 \times PV_{meso}/SA$.
[d] Volume of pores larger than 50 nm in diameter.
[e] Peak in pore size distribution on micrometer scale.
[f] Amounts of probe molecules adsorbed at 200°C in the TPD measurement.
[g] Apparent first-order reaction rate constant in the cracking of cumene at 300°C.

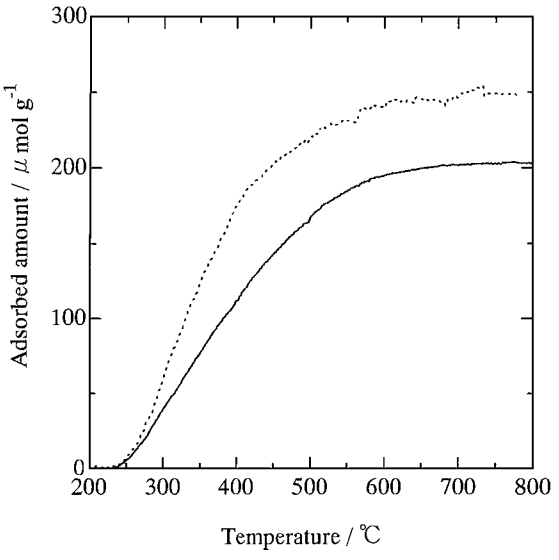

FIG. 5. TPD profiles of NH_3 (dotted line) and 2,6-DMP (solid line) adsorbed on the sample of SAO3 at 200°C.

structure of aluminum in silica networks, leading to the generation of a large number of Brønsted acid sites. Because there remains uncertainty in the relation between structure of silica–alumina and acidic properties, it is difficult to clarify how PEO aids in the generation of Brønsted acid sites. Miller *et al.* have shown that use of organic chelating reagents in the preparation of silica–zirconia increases the homogeneity in the resultant gel [19]. They related the effect of additives to the matching reactivities of the TEOS and zirconium alkoxide reactants in sol–gel reactions. In addition, organic additives may also improve the uniformity of metal oxides by affecting the structure formation pathways in sol–gel reactions (28) and structural evolution during drying and heating (27, 29).

In the catalytic test of silica–alumina for the cracking of cumene (Table 2), samples with macropores show high activity. The reaction rate well correlates with the number of Brønsted acid sites estimated by TPD measurements. Namely, the Brønsted acid sites formed by the aid of the presence of PEO work effectively in the cracking of cumene. Here, we could not prove the effectivity of the presence of the macropores in the laboratory-scale reactor, because the catalyst had been powdered before the catalytic test. The usefulness of macropores becomes particularly important in industrial applications, where the catalysts are used in various forms such as rod, sphere, and cylinder. The present procedure for preparing silica–alumina with bimodal pore structures can directly provide a catalyst with monolithic form with an appropriate shape without any posttreatments, such as granulation and molding using some binders. In our future work, we will investigate the effectiveness of the bicontinuous macropore morphology in catalysis.

CONCLUSIONS

A silica–alumina with distinct bimodal pore structure was prepared by phase separation in sol–gel reactions of TEOS and aluminum nitrate in the presence of PEO. It contains continuous macropores with uniform size between 0.3 and 5 μm. It was found that the macropore size changes with the compositions in sol–gel reactions. The macropores are formed by fixing transitional structures of spinodal decomposition by gelation. Here, the size of the pore changes depending on the timing of the onset of the spinodal decomposition and gelation. The change in the starting composition would affect the timing. The silica–alumina prepared with PEO has a large number of Brønsted acid sites effective for the cracking of cumene, probably because the PEO increases the uniformity of Al atoms in the silica network which would be a cause of the formation of Brønsted acid sites.

ACKNOWLEDGMENT

The authors thank Professor Kazuki Nakanishi, Kyoto University, Japan, for his advice on morphology control and cooperation in measurement of pore size distribution with mercury porosimetry.

REFERENCES

1. Wakao, N., and Smith, J. M., *Chem. Eng. Sci.* **17**, 825 (1962).
2. Nakanishi, K., and Soga, N., *J. Am. Ceram. Soc.* **74**, 2518 (1991).
3. Nakanishi, K., Komura, H., Takahashi, R., and Soga, N., *Bull. Chem. Soc. Japan* **67**, 1327 (1994).
4. Nakanishi, K., *J. Porous Mater.* **4**, 67 (1997).
5. Minakuchi, H., Nakanishi, K., Soga, N., Ishizuka, N., and Tanaka, N., *Anal. Chem.* **68**, 3498 (1996).
6. Tanabe, K., Misono, M., Ono, Y., and Hattori, H., *Stud. Surf. Sci. Catal.* **51**, 116 (1989).
7. Sato, S., Toita, M., Yu, Y. Q., Sodesawa, T., and Nozaki, F., *Chem. Lett.*, 1535 (1987).
8. Sato, S., Toita, M., Sodesawa, T., and Nozaki, F., *Appl. Catal.* **62**, 73 (1990).
9. Sato, S., Sodesawa, T., Nozaki, F., and Shoji, H., *J. Mol. Catal.* **66**, 343 (1991).
10. Jin, T., Okuhara, T., and White, J. M., *J. Chem. Soc. Chem. Commun.*, 1248 (1987).
11. Niwa, M., Katada, N., and Murakami, Y., *J. Catal.* **134**, 340 (1992).
12. Katada, N., and Niwa, M., *Chem. Vap. Deposition* **2**, 125 (1996).
13. Sheng, T.-C., and Gay, I. D., *J. Catal.* **145**, 10 (1994).
14. Ueno, A., Suzuki, H., and Kotera, Y., *J. Chem. Soc. Faraday Trans.* **79**, 127 (1983).
15. Cauqui, M. A., and Rodoriguez-Izquierdo, J. M., *J. Non-Cryst. Solids* **147/148**, 724 (1992).
16. Zou, W., and Gonzalez, R., *J. Catal.* **152**, 291 (1995).
17. Takahashi, R., Sato, S., Sodesawa, T., Kato, M., and Yoshii, T., *Chem. Lett.*, 305 (1999).
18. Toba, M., Mizukami, F., Niwa, S., and Maeda, K., *J. Chem. Soc. Chem. Commun.*, 1211 (1990).
19. Miller, J., Rankin, S., and Ko, E., *J. Catal.* **148**, 673 (1994).
20. Miller, J., and Ko, E., *J. Catal.* **159**, 83 (1996).
21. Dollimore, D., and Heal, G. R., *J. Appl. Chem.* **14**, 109 (1964).

22. Sato, S., Tokumitsu, M., Sodesawa, T., and Nozaki, F., *Bull. Chem. Soc. Japan* **64**, 1005 (1991).
23. Sato, S., Takematsu, K., Sodesawa, T., and Nozaki, F., *Bull. Chem. Soc. Japan* **65**, 1486 (1992).
24. Sato, S., Kuroki, M., Sodesawa, T., Nozaki, F., and Maciel, G. E., *J. Mol. Catal. A* **104**, 171 (1995).
25. Basett, D. W., and Habgood, H. W., *J. Phys. Chem.* **64**, 769 (1960).
26. Kingery, W. D., Bowen, H. K., and Uhlmann, D. W., *in* "Introduction to Ceramics," 2nd ed., Chap. 8, p. 320. Wiley, New York, 1976.
27. Takahashi, R., Nakanishi, K., and Soga, N., *Faraday Discuss.* **101**, 249 (1995).
28. Takahashi, R., Nakanishi, K., and Soga, N., *J. Sol–Gel Sci. Technol.* **17**, 7 (2000).
29. Takahashi, R., Sato, S., Sodesawa, T., Suzuki, M., and Ogura, K., *Bull. Chem. Soc. Japan* **73**, 765 (2000).